Carbon 157 (2020) 364–370

Contents lists available at ScienceDirect

Carbon

journal homepage: www.elsevier.com/locate/carbon

# In-plane breathing and shear modes in low-dimensional nanostructures

Dan Liu [a], Colin Daniels [b], Vincent Meunier [b], Arthur G. Every [c], David Tománek [a, *]

[a] Physics and Astronomy Department, Michigan State University, East Lansing, MI, 48824, USA
[b] Department of Physics, Applied Physics, and Astronomy, Rensselaer Polytechnic Institute, Troy, NY, 12180, USA
[c] School of Physics, University of the Witwatersrand, Private Bag 3, 2050, Johannesburg, South Africa

ARTICLE INFO

*Article history:*
Received 25 September 2019
Received in revised form
11 October 2019
Accepted 17 October 2019
Available online 22 October 2019

*Keywords:*
Radial breathing mode
RBM
2D
Raman
DFT
*ab initio*
Graphene nanoribbon

ABSTRACT

We use continuum elasticity theory to revise scaling laws for radial breathing-like and shear-like vibration modes in quasi-2D nanostructures including finite-width nanoribbons and finite-size thin circular discs. Such modes can be observed spectroscopically in corresponding nanostructures of graphene and phosphorene and can be determined numerically by atomistic *ab initio* density functional theory and classical force-field calculation. The revised scaling laws differ from previously used expressions, some of which display an unphysical asymptotic behavior. Apart from model assumptions describing the effect of edge termination, the continuum scaling laws have no adjustable parameters and display correct asymptotic behavior. These scaling laws yield excellent agreement with experimental and numerical results for vibration frequencies in both isotropic and anisotropic structures as well as useful expressions for the frequency dependence on structure size and edge termination.



## 1. Introduction

Well-defined nanostructures of carbon and other elements, including the $C_{60}$ buckyball [1] and other fullerenes, carbon nanotubes [2], and graphene nanoribbons [3] have been produced with atomic-scale precision [4]. Resonant Raman spectroscopy has emerged as the most powerful method to identify and characterize each of these nanostructures within a sample. There are extensive theoretical and experimental studies [5–8] that relate the frequency $\omega_{RBM}$ of the radial breathing mode (RBM) of carbon fullerenes and nanotubes to their diameter. In turn, the diameter of these nanostructures can be inferred from Raman spectra.

For finite-width 2D nanoribbons, several theoretical studies utilized time-consuming atomistic total energy calculations and translated frequency results to frequency-width scaling laws [9–12] that displayed an unphysical asymptotic behavior for wide nanoribbons. Other studies [13–15] obtained the correct asymptotic behavior for wide nanoribbons using the Brillouin zone folding approach, but could not find agreement with experimental data in narrow nanoribbons.

With precision rivaling that of *ab initio* calculations at much lower computational effort, RBM frequencies of near-spherical fullerenes and cylindrical nanotubes have been obtained by representing these nanostructures by elastic membranes characterized by 2D elastic constants [16]. In the standard Voigt notation, adapted to a 2D solid [16], these yield

$$\omega_{C_n} = \frac{2}{d}\sqrt{\frac{2c_{11}}{\rho_{2D}}}, \tag{1}$$

for the RBM frequency of a spherical $C_n$ fullerene with diameter $d$. Similarly, the RBM frequency of a carbon nanotube (CNT) of radius $d$ is given by

$$\omega_{CNT} = \frac{2}{d}\sqrt{\frac{c_{11}}{\rho_{2D}}}. \tag{2}$$

The planar counterpart of a cylindrical CNT is an infinite, planar nanoribbon of width $W$. In analogy, planar circular nanodiscs of radius $R$ are planar counterparts of spherical fullerenes.

Here we present continuum elasticity theory results that translate into revised scaling laws for radial breathing-like and

* Corresponding author.
*E-mail address:* tomanek@pa.msu.edu (D. Tománek).

https://doi.org/10.1016/j.carbon.2019.10.041
0008-6223/

shear-like vibration modes in quasi-2D nanostructures including finite-width nanoribbons and finite-size thin circular discs. Such modes have been observed spectroscopically in corresponding nanostructures of graphene and phosphorene and can be determined numerically by atomistic *ab initio* density functional theory and classical force-field calculation. The revised scaling laws differ from previously used expressions, some of which display an unphysical asymptotic behavior in wide nanostructures. Apart from model assumptions describing the effect of edge termination, the continuum scaling laws have no adjustable parameters and display correct asymptotic behavior. These scaling laws yield excellent agreement with experimental and numerical results for vibration frequencies in both isotropic and anisotropic structures as well as useful expressions for the frequency dependence on structure size and edge termination.

## 2. Analytical scaling laws

### 2.1. Expressions for breathing-like and shear-like modes of nanoribbons

Let us first consider an infinitely long nanoribbon of width $W$ and 2D mass density $\rho_{2D}$, represented in Fig. 1 (a), which is free of tensile strain energy. To obtain an expression for the in-plane radial breathing-like mode (RBLM), we first consider two longitudinal acoustic (LA) waves propagating in opposite direction within an infinite layer with velocity $v = \omega/k$, producing a standing wave with $\lambda = 2\pi/k$ as interference pattern. This pattern is an array of infinitely long strips, separated by stress nodal lines $\lambda/2$ apart. Cutting the plane along adjacent stress nodal lines of the standing wave, which are immobile in the plane, will produce a ribbon of finite width $W = \lambda/2$ that will vibrate with the same frequency $\omega$ if edge effects can be ignored. 2D continuum elasticity theory calculations provide the expression [16].

$$\omega_{LA}(k) = \sqrt{\frac{c_{11}}{\rho_{2D}}}\, k \tag{3}$$

for the LA mode of the infinite layer corresponding to the in-plane breathing-like mode of a nanoribbon. Substituting $k = 2\pi/\lambda = 2\pi/(2W)$ from above in Eq. (3), we obtain

$$\omega_{RBLM,0} = \frac{\pi}{W}\sqrt{\frac{c_{11}}{\rho_{2D}}} \tag{4}$$

for the RBLM frequency $\omega_{RBLM,0}$ that ignores any edge effects. A similar expression has been derived previously [13–15] using the Brillouin zone folding approach based on the phonon spectrum of an infinite monolayer. In an anisotropic material, $c_{11}$ has to be replaced by the elastic constant associated with the direction normal to the nanoribbon axis.

In nanoribbons with bare edges, the width $W$ is defined by the distance between atoms at opposite edges. Most experiments, however, are performed not on bare, but rather chemically terminated nanoribbons. Chemical functionalization, such as H- or OH-termination of graphene edges, changes the elastic response at the edge. More important, it effectively increases the width $W$ and mass of the nanoribbon by a constant amount per length of the nanoribbon. Both latter effects lower the frequency of the RBLM mode and can be accommodated by effectively increasing the bare width $W$ by $\delta W$ in Eq. (4). The value of $\delta W$ will represent changes in the edge region with respect to the nanoribbon material. $\delta W$ should not change when the nanoribbon width changes.

In view of these considerations, the scaling law of Eq. (4) should be modified to

$$\omega_{RBLM} = \frac{c_{RBLM}}{W + \delta W} \tag{5}$$

$$\text{with } c_{RBLM} = \pi\sqrt{\frac{c_{11}}{\rho_{2D}}},$$

where edge effects are described by $\delta W$ as the only adjustable parameter. The effect of specific edge terminations on $\omega_{RBLM}$ will be discussed later on.

We note that the functional dependence of $\omega_{RBLM}$ on the nanoribbon width $W$ in Eq. (5) differs significantly from the previously used expression [9–11] $\omega_{RBLM} = a/\sqrt{W} + b$, where $a \approx 1.6 \times 10^3$ cm$^{-1}$ Å$^{1/2}$ and $b \approx -2 \times 10^2$ cm$^{-1}$ have been obtained by numerical fits to observed and calculated frequencies for a finite range of widths, with the asymptotic behavior $\omega_{RBLM} \approx -2 \times 10^2$ cm$^{-1}$ for $W \to \infty$. An alternative expression [12] $\omega_{RBLM} = c/W + d/\sqrt{W} +$

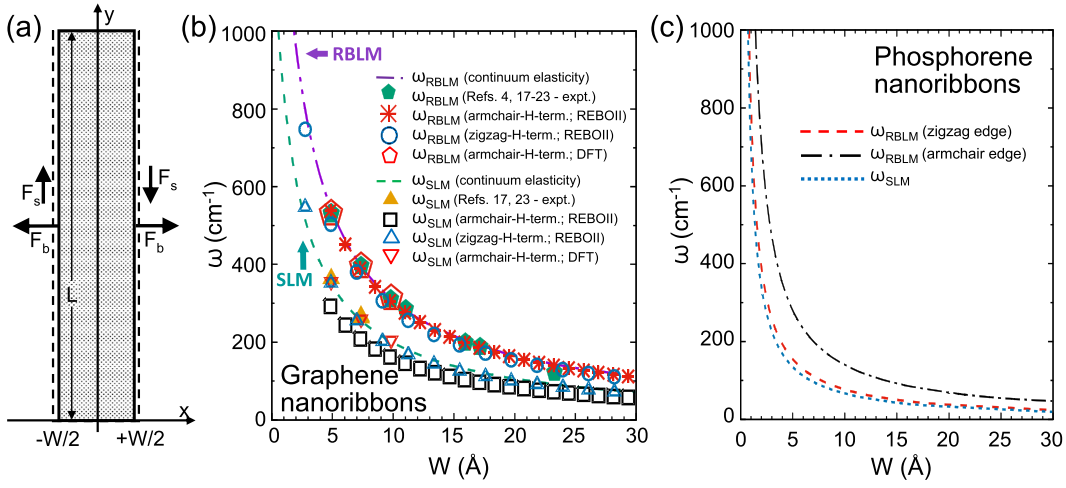


**Fig. 1.** In-plane breathing-like and shear-like modes of an infinite planar nanoribbon of bare width $W$. (a) Schematic of the deformations considered here. (b) Numerical results for the $W$-dependence of the radial breathing-like mode frequency $\omega_{RBLM}$ and the shear-like mode (SLM) frequency $\omega_{SLM}$ in armchair graphene nanoribbons (aGNRs) using the continuum elasticity and atomistic approaches. (c) Continuum elasticity results for the $W$-dependence of $\omega_{RBLM}$ and $\omega_{SLM}$ in phosphorene nanoribbons cut along the softer direction 1 or the harder direction 2. Experimental data are reproduced from Refs. [4,17–23]. (A colour version of this figure can be viewed online.)

$e$, with $c \approx 1.6 \times 10^3$ cm$^{-1}$ Å, $d \approx 4 \times 10^2$ cm$^{-1}$ Å$^{1/2}$ and $e = -10$ cm$^{-1}$, has been proposed subsequently for an extended range of nanoribbon widths, with the asymptotic behavior $\omega_{RBLM} = -10$ cm$^{-1}$ for $W \to \infty$. The asymptotic behavior is clearly incorrect in both expressions, since it should approach zero for $W \to \infty$. Comparison of the dependence of $\omega_{RBLM}$ using the different expressions is provided in the Supplemental Material (SM) [24].

Similar to Eqs. (4) and (5) for the RBLM of a nanoribbon, we can describe the shear-like mode (SLM) frequency of the same nanoribbon by [16].

$$\omega_{SLM,0} = \frac{\pi}{W}\sqrt{\frac{c_{66}}{\rho_{2D}}} \tag{6}$$

in analogy to the in-plane transverse acoustic (TA) mode in the infinite layer.

We describe the effect of edge termination on the SLM modes in the same way as on the RBLM mode in the expression

$$\omega_{SLM} = \frac{c_{SLM}}{W + \delta W}, \qquad c_{SLM} = \pi\sqrt{\frac{c_{66}}{\rho_{2D}}}. \tag{7}$$

The value of $\delta W$ is the same as in Eq. (5). The effect of specific edge terminations on $\omega_{SLM}$ will be discussed later on.

### 2.2. Expression for the in-plane breathing mode of thin circular discs based on 2D continuum elasticity theory

Continuum elasticity theory allows to calculate the frequency of the radial breathing mode $\omega_{RBM}$ of a solid sphere of radius $R$, consisting of a uniform, isotropic material of mass density ρ, with the help of elastic constants $C_{ij}$, including the related bulk modulus $B$. In a similar way, the 2D bulk modulus γ and other 2D elastic constants $c_{ij}$ should provide a useful expression for $\omega_{RBM}$ of a massive circular disc of radius $R$ and mass density $\rho_{2D}$, which could be measured by Raman spectroscopy. While $\omega_{RBM}$ depends independently on both $c_{11}$ and $c_{12}$, it is particularly sensitive to the 2D bulk modulus $\gamma = (c_{11} + c_{12})/2$ described below.

Extensive atomistic calculations of the 2D bulk modulus γ of graphene and a number of other isotropic quasi-2D solids have been reported previously [26]. The 2D bulk modulus, also known as "membrane stretching modulus" or "area-stretching elastic constant", is a measure of the elastic resistance of a 2D solid to change in the area under isotropic line force $F$ applied in the two in-plane directions. We found one available expression for γ, published in Ref. [26], to be incorrect, apparently due to the faulty assumption that an isotropic stress results in an isotropic strain. In the following we derive the correct expression for the 2D bulk modulus γ of an anisotropic solid.

#### 2.2.1. Continuum elasticity expression for the 2D bulk modulus of an anisotropic material

Consider a finite-size square object that is cut out of a generally anisotropic 2D solid and subject to uniform tensile stress $P = \sigma_{11} = \sigma_{22}$ in the in-plane directions, as shown in Fig. 2. The stress $P = F/L$, caused by an external force $F$ acting on side length $L$, is the 2D counterpart of uniform pressure, and causes a fractional change in area, or areal strain $\delta A/A = \varepsilon_{11} + \varepsilon_{22}$. There are no shear stresses, and any shear strain $\varepsilon_{12}$ does not contribute to a change in the area, and so is not shown in Fig. 2. In the standard Voigt notation, adapted to a 2D solid [16], the stress-strain relationship takes the form

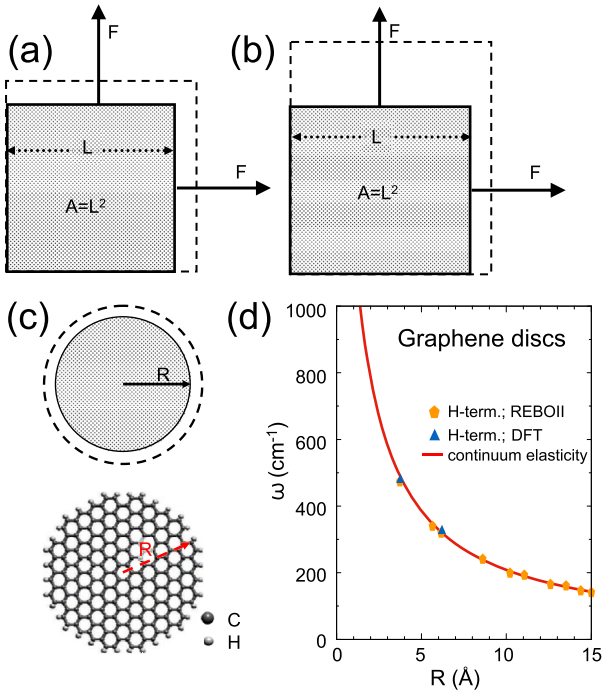


**Fig. 2.** In-plane deformation of a finite-size planar flake in the initial shape of a square of side length $L$ for an (a) isotropic and (b) anisotropic material. (c) Schematic radial motion in a thin circular disc of radius $R$ and a ball-and-stick representation of a graphene disc. (d) Continuum elasticity results for the $R$-dependence of $\omega_{RBM}$ in a graphene disc with H-terminated edges. The data points are results of atomistic calculations using the REBOII [25] force-field. (A colour version of this figure can be viewed online.)

$$\begin{pmatrix}\varepsilon_{11}\\ \varepsilon_{22}\\ \varepsilon_{12}\end{pmatrix} = \begin{pmatrix}s_{11} & s_{12} & s_{16}\\ s_{12} & s_{22} & s_{26}\\ s_{16} & s_{26} & s_{66}\end{pmatrix}\begin{pmatrix}P\\ P\\ 0\end{pmatrix}, \tag{8}$$

where $s_{ij}$ are the 2D compliance constants, which form a symmetric matrix. It follows that the areal extensibility $k$, the 2D counterpart of 3D compressibility, is given by

$$k = \frac{\delta A}{A}\cdot\frac{1}{P} = \frac{\varepsilon_{11} + \varepsilon_{22}}{P} = s_{11} + s_{22} + 2s_{12}. \tag{9}$$

The 2D bulk modulus γ is the inverse of the extensibility, so that

$$\gamma = \frac{1}{k} = \frac{1}{s_{11} + s_{22} + 2s_{12}}. \tag{10}$$

For 2D structures, the elastic stiffness constants $c_{ij}$ are in more common use than the compliance constants [16], so it is useful to be able to express the bulk modulus in terms of stiffness constants. In principle this is straightforward since the stiffness and compliance matrices are the inverse of each other. For general anisotropy, numerical inversion seems the most viable option. Of more practical importance, for square, hexagonal and rectangular structures, $s_{16} = s_{26} = 0$ and $c_{16} = c_{26} = 0$, and the required inverted compliance constants are readily obtained as

$$s_{11} = \frac{c_{22}}{c_{11}c_{22} - c_{12}^2} ,$$
$$s_{12} = \frac{-c_{12}}{c_{11}c_{22} - c_{12}^2} , \quad (11)$$
$$s_{22} = \frac{c_{11}}{c_{11}c_{22} - c_{12}^2} .$$

Inserting these expressions in Eq. (10), one arrives at

$$\gamma = \frac{c_{11}c_{22} - c_{12}^2}{c_{11} + c_{22} - 2c_{12}} . \quad (12)$$

For an isotropic solid with $c_{11} = c_{22}$, Eq. (12) reduces to

$$\gamma = \frac{1}{2}(c_{11} + c_{12}) . \quad (13)$$

*2.2.2. Continuum elasticity description of in-plane vibrations in circular discs*

In-plane vibrations of circular discs have been extensively discussed in the literature, including Ref. [27] and references cited therein. The fundamental frequency is readily obtained from the equation for the radial modes of an isotropic cylinder, which can be found e.g. in Rose's book [28]. Setting $k$ along the axis to zero and dividing the right-hand side by 2, the cylinder equation reduces to

$$J_1\left(\frac{\omega_{RBM}R}{v_{LA}}\right) = \left(\frac{\omega_{RBM}Rv_{LA}}{2v_{TA}^2}\right)J_0\left(\frac{\omega_{RBM}R}{v_{LA}}\right) , \quad (14)$$

where $J_0$ and $J_1$ are Bessel functions and $R$ is the radius of the cylinder. This equation applies equally to the radial modes of a thin disc, requiring only that $v_{LA} = \sqrt{c_{11}/\rho_{2D}}$ be treated as the 2D longitudinal acoustic velocity and $v_{TA} = \sqrt{c_{66}/\rho_{2D}}$ as the transverse acoustic velocity. Remembering that $c_{66} = (c_{11} - c_{12})/2$ in an isotropic 2D material [16] we consider here, we can further define $x = \omega_{RBM}R/v_{LA}$ and rewrite Eq. (14) as

$$J_1(x) = CxJ_0(x) . \quad (15)$$

Here, $C = c_{11}/(2\gamma)(c_{11} + c_{12})/(c_{11} - c_{12}) = c_{11}/(c_{11} - c_{12})$ is a constant depending on the elastic constants of the material. According to its definition, the root of Eq. (15) is related to the fundamental frequency of a circular isotropic disc by $x = \omega_{RBM}R\sqrt{\rho_{2D}/c_{11}}$, so that

$$\omega_{RBM} = \frac{x}{R}\sqrt{\frac{c_{11}}{\rho_{2D}}} . \quad (16)$$

The general solution of Eq. (15) has to be obtained numerically for a given material and provides both the fundamental frequency and the overtones.

In the following, we will apply the above expressions for the different vibration mode frequencies to specific nanostructures, in particular nanoribbons and thin circular discs formed of 2D graphene and phosphorene.

## 3. Numerical results for specific materials and structures

### 3.1. Nanoribbons of graphene and phosphorene

Our results for $\omega_{RBLM}$ and $\omega_{SLM}$ for armchair graphene nanoribbons (aGNRs) are presented in Fig. 1(b). Graphene is isotropic and characterized by [16] $c_{11} = c_{22} = 352.6$ N/m, $c_{12} = 59.6$ N/m, $c_{66} = 146.5$ N/m, and $\rho_{2D} = 0.743 \times 10^{-6}$ kg/m$^2$. The width of bare $N$-aGNRs is given by Ref. [3] $W = (N-1) \times 1.23$ Å and the width of $N$-zGNRs with a zigzag edge is given by $W = (2.13N - 1.42)$ Å.

Whereas bare edges are known to reconstruct and change their elastic response, chemical termination adds width and mass to the edge. Graphene edges are often terminated by H- or OH- groups in aqueous environment [29]. Considering only the width change in case of hydrogen-terminated GNRs, we may expect $\delta W \approx 2.2$ Å in view of the typical C–H bond length of 1.1 Å at the edges. As seen in Fig. 3, we found that all data for $\omega_{RBLM}$ in H-terminated GNRs, whether obtained spectroscopically or by atomistic calculations, could be reproduced accurately by continuum elasticity theory Eqs. (5) and (7) using the value $\delta W = 1.8$ Å for H-termination, which agrees in the order of magnitude with our estimate. For OH-terminated edges, continuum elasticity calculations using $\delta W = 5.5$ Å reproduce well numerical results for $\omega_{RBLM}$ and $\omega_{SLM}$ as seen in Fig. 3. Clearly, the higher mass of the OH- termination is reflected in a larger value of $\delta W$. Due to the isotropy of graphene, the vibration frequencies are the same for armchair and zigzag nanoribbons of the same width, as confirmed by results of our atomistic calculations presented in Fig. 1(b).

Unlike graphene, phosphorene is anisotropic and characterized by [16] $c_{11} = 24.4$ N/m, $c_{22} = 94.6$ N/m, $c_{12} = 7.9$ N/m, $c_{66} = 22.1$ N/m, and $\rho_{2D} = 1.34 \times 10^{-6}$ kg/m$^2$. This anisotropy is reflected in our results for $\omega_{RBLM}$ and $\omega_{SLM}$ for armchair and zigzag phosphorene nanoribbons, presented in Fig. 1(c).

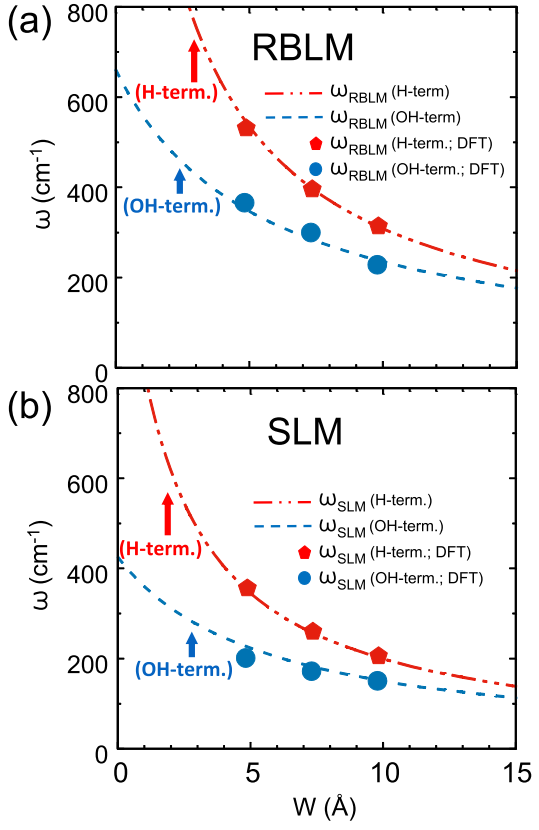


**Fig. 3.** Effect of edge termination on vibration modes in GNRs. Results for (a) $\omega_{RBLM}$ and (b) $\omega_{SLM}$ obtained using Eq. (5) are presented for edge termination by either lighter H- or heavier –OH groups. (A colour version of this figure can be viewed online.)

### 3.2. Thin circular discs of graphene

Using Eq. (13) for isotropic media and the above-mentioned elastic constants for graphene [16], we obtain the value $\gamma = 206.1$ N/m for the 2D bulk modulus of graphene, in agreement with previously published results [26]. With $C = c_{11}/(c_{11} - c_{12}) = 352.6/(352.6 - 59.6) = 1.203$, the solution of Eq. (15) is $x = 1.963$. The dependence of the fundamental frequency $\omega_{RBM}$ in thin circular discs on their radius $R$ is then given by Eq. (16) and presented in Fig. 2(d). Atomic displacements during the radial breathing modes of these discs are displayed in the SM [24].

Results of atomistic calculations for hydrogen-terminated discs based on DFT and the REBOII force field [25] are compared to continuum results in Fig. 2(d). General agreement between continuum and atomistic results provides strong support for the universal nature of Eq. (16) to correctly represent $\omega_{RBM}$ of thin circular discs. Similar to bare and chemically terminated nanoribbons, the narrow region near the edge is not represented well by continuum elasticity theory due to changes in width, mass distribution and local elastic behavior. Like in the case of nanoribbons, we accommodate these effects in a single parameter $\delta R$ that modifies the radius $R$ of the thin circular disc. We found good agreement between atomistic and continuum results using $\delta R = 0.9$ Å and note that this value agrees with $\delta W/2$ used earlier for hydrogen-terminated nanoribbons.

## 4. Discussion

We found the accuracy of the 2D elasticity approach and its ability to correctly represent vibration modes down to the nanometer scale to be impressive, but not completely unexpected in view of published results for acoustic, in particular flexural modes of 2D materials and systems like carbon fullerenes and nanotubes [16]. More important in our view is the fact that this approach provides a physically motivated expression for RBLM and SLM modes in nanoribbons in Eqs. (5) and (7), which differs from the established form and does not suffer from an asymptotically incorrect behavior for ultra-wide nanoribbons. In addition, by relating the frequency to intrinsic elastic properties of the material, the provided expressions offer a wide range of applicability for 2D nanostructures of any layered material.

Furthermore, even though many 2D materials such as graphene are isotropic, some are not, with black phosphorene being a notable example. As seen in Fig. 1(c), the vibration frequencies of phosphorene nanoribbons depend sensitively on whether their edges are along the zigzag or the armchair direction, and this behavior can be described by the same continuum elasticity theory.

Chemical termination of edges poses, of course, a problem for the continuum description of finite-size objects. Depending on the termination type, the edge region will have a different mass distribution, different elastic behavior, and will add a nonzero width $\delta W$ to finite-size objects. We believe that the value of $\delta W$ in nanoribbons and the corresponding value $\delta R = \delta W/2$ in thin circular discs, which we used in our study, describes adequately the combined effect of elastic softening near the edge and, in case of chemical termination, an increase of the width and mass of the nanostructure. We should also note that the effect of chemical termination should be different for terminating H-, O- and OH-groups.

One of the chemical edge termination effects, namely the addition of atomic masses at the edge, can be treated analytically, as shown in the Appendix. We find that in many cases, including nanoribbons and thin circular discs, keeping $\delta W$ and $\delta R$ as an adjustable parameter that is independent of $W$ or $R$ provides satisfactory results especially for wide nanostructures. In systems, where the termination size is similar to the size of the nano-object, continuum elasticity treatment loses its justification.

Our calculations are all for natural normal modes of nanostructures, whether nanoribbons or thin circular discs. We wish to note that these vibrations differ from forced modes that may be induced by applying strain in a particular way. A nanoribbon may be stretched uniformly normal to its axis by applying constant 2D tensile strain along the edges. Releasing this strain results in a soft vibration mode with a frequency higher by the factor $\sqrt{12}/\pi$ than the eigenmode described by Eq. (4). This reveals that this particular forced mode is not an eigenmode, but rather a mixed mode of the nanoribbon.

## 5. Summary and conclusions

We have used 2D continuum elasticity theory and atomistic calculations to determine in-plane radial breathing-like and shear-like vibration modes of low-dimensional nanostructures including finite-width nanoribbons and finite-size thin circular discs of graphene and phosphorene. These vibrations can be observed by Raman spectroscopy and used to characterize the sample. Vibrational modes are sensitive not only to shape and mass density, but also to anisotropy in the elastic behavior. We have derived revised scaling laws that differ from previously used expressions, some of which display an unphysical asymptotic behavior in wide nanostructures. Apart from model assumptions describing the effect of edge termination, the continuum scaling laws have no adjustable parameters and display correct asymptotic behavior. These scaling laws yield excellent agreement with experimental and numerical results for vibration frequencies in both isotropic and anisotropic structures as well as useful expressions for the frequency dependence on structure size and edge termination.

## Declaration of competing interest

The authors declare that they have no known competing financial interestsor personal relationships that could have appeared to influence the work reported in this paper.

## Acknowledgments

DL and DT acknowledge partial support by the NSF/AFOSR EFRI 2-DARE grant number EFMA-1433459. DT also acknowledges support by the Mandelstam Institute for Theoretical Physics (MITP) and the Simons Foundation, award number 509116.

## 6. Appendix

### 6.1. Description of Nanoribbons with Massive Edge Termination

An alternative way to describe the effect of edge termination is to rigidly attach a line of constant mass density both edges. To see its effect, let us first consider the nanoribbon of width $W$ in Fig. 1 that lies in the $x-y$ plane, with its axis aligned with the $y-$ direction. Breathing modes of the ribbon, which are LA waves with $\mathbf{k}$ normal to the length of the ribbon, can be classified as symmetric or anti-symmetric with respect to the midline of the ribbon. Both are required to satisfy the wave equation for the medium and the boundary conditions at the edges. In the case of symmetric modes, for which the motions of mass elements in the nanoribbon are related by $u(x,t) = -u(-x,t)$, solutions of the wave equation take the form

$$u(x,t) = A\sin(kx)e^{i\omega t} \tag{A1}$$

with ω and $k = |\mathbf{k}|$ related by the dispersion relation

$$\omega = \sqrt{\frac{c_{11}}{\rho_{2D}}}\,k\,, \tag{A2}$$

which is identical to Eq. (3). In the case of antisymmetric modes for which $u(x,t) = u(-x,t)$, the form of the wave equation changes to

$$u(x,t) = A\cos(kx)e^{i\omega t} \tag{A3}$$

with the same dispersion relation (A2). We now consider a line of constant mass density μ representing mass per length to be rigidly connected to the edges at $x = -W/2$ and $x = +W/2$.

To determine $k$ and ω, we have to impose the boundary condition

$$\sigma_x\left(\pm\frac{W}{2}\right) = \mu a_x\,, \tag{A4}$$

where $\sigma_x(\pm W/2)$ is the tensile stress at $\pm W/2$ and $a_x$ is the acceleration. This leads to

$$c_{11}\frac{\partial u}{\partial x} = -\mu\frac{\partial^2 u}{\partial t^2} \tag{A5}$$

at the edges $x = \pm W/2$, where the negative sign indicates that the stretch pulls the mass at the edge inward. Inserting expression (A1) into Eq. (A5) for symmetric modes leads to

$$kc_{11}\cos\left(k\frac{W}{2}\right) = \mu\omega^2\sin\left(k\frac{W}{2}\right)\,. \tag{A6}$$

To eliminate the quantity $k$, we insert expression (A2) into Eq. (A6) and obtain

$$\omega c_{11}\sqrt{\frac{\rho_{2D}}{c_{11}}}\cos\left(\omega\frac{W}{2}\sqrt{\frac{\rho_{2D}}{c_{11}}}\right) = \mu\omega^2\sin\left(\omega\frac{W}{2}\sqrt{\frac{\rho_{2D}}{c_{11}}}\right)\,. \tag{A7}$$

This can be simplified to the transcendental equation

$$\tan\left(\omega\frac{W}{2}\sqrt{\frac{\rho_{2D}}{c_{11}}}\right) = \frac{c_{11}}{\mu\omega}\sqrt{\frac{\rho_{2D}}{c_{11}}}\,. \tag{A8}$$

In the limiting case of no additional mass at the edge or $\mu = 0$, the right-hand side of Eq. (A8) diverges and the argument of the tangent-function becomes $\pi/2$. The fundamental frequency is given by

$$\omega\frac{W}{2}\sqrt{\frac{\rho_{2D}}{c_{11}}} = \frac{\pi}{2}\,, \tag{A9}$$

which translates to Eq. (4) for $\omega_{RBLM}$. In the limiting case of an infinitely heavy edge with $\mu\to\infty$, the right-hand side of Eq. (A8) vanishes. For the fundamental frequency we then obtain

$$\omega\frac{W}{2}\sqrt{\frac{\rho_{2D}}{c_{11}}} = \pi\,. \tag{A10}$$

The calculation for antisymmetric modes follows along similar lines and yields

$$\cot\left(\omega\frac{W}{2}\sqrt{\frac{\rho_{2D}}{c_{11}}}\right) = -\frac{c_{11}}{\mu\omega}\sqrt{\frac{\rho_{2D}}{c_{11}}}\,. \tag{A11}$$

The limiting cases are $\mu = 0$, described by Eq. (A10), and $\mu\to\infty$, described by Eq. (A9).

## Supplementary data

Supplementary data to this article can be found online at https://doi.org/10.1016/j.carbon.2019.10.041.

## References


[1] H.W. Kroto, J.R. Heath, S.C. O'Brien, R.F. Curl, R.E. Smalley, $C_{60}$: buckminsterfullerene, Nature 318 (6042) (1985) 162–163, https://doi.org/10.1038/318162a0.

[2] S. Iijima, Helical microtubules of graphitic carbon, Nature 354 (6348) (1991) 56–58, https://doi.org/10.1038/354056a0.

[3] D. Tománek, Guide through the Nanocarbon Jungle, IOP Publishing, Bristol, UK, 2014. https://doi.org/10.1088/978-1-627-05273-3.

[4] J. Cai, P. Ruffieux, R. Jaafar, M. Bieri, T. Braun, S. Blankenburg, M. Muoth, A.P. Seitsonen, M. Saleh, X. Feng, K. Müllen, R. Fasel, Atomically precise bottom-up fabrication of graphene nanoribbons, Nature 466 (2010) 470, https://doi.org/10.1038/nature09211.

[5] A.M. Rao, E. Richter, S. Bandow, B. Chase, P.C. Eklund, K.A. Williams, S. Fang, K.R. Subbaswamy, M. Menon, A. Thess, R.E. Smalley, G. Dresselhaus, M.S. Dresselhaus, Diameter-selective Raman scattering from vibrational modes in carbon nanotubes, Science 275 (5297) (1997) 187–191, https://doi.org/10.1126/science.275.5297.187. https://science.sciencemag.org/content/275/5297/187.

[6] H. Suzuura, T. Ando, Phonons and electron-phonon scattering in carbon nanotubes, Phys. Rev. B 65 (2002) 235412, https://doi.org/10.1103/PhysRevB.65.235412. http://link.aps.org/doi/10.1103/PhysRevB.65.235412.

[7] A.C. Ferrari, J. Robertson, H. Kuzmany, R. Pfeiffer, M. Hulman, C. Kramberger, Raman spectroscopy of fullerenes and fullerene-nanotube composites, Philos. Trans. R. Soc. A Math. Phys. Eng. Sci. 362 (1824) (2004) 2375–2406, https://doi.org/10.1098/rsta.2004.1446. https://royalsocietypublishing.org/doi/abs/10.1098/rsta.2004.1446.

[8] J. Maultzsch, H. Telg, S. Reich, C. Thomsen, Radial breathing mode of single-walled carbon nanotubes: optical transition energies and chiral-index assignment, Phys. Rev. B 72 (2005) 205438, https://doi.org/10.1103/PhysRevB.72.205438. https://link.aps.org/doi/10.1103/PhysRevB.72.205438.

[9] J. Zhou, J. Dong, Vibrational property and Raman spectrum of carbon nanoribbon, Appl. Phys. Lett. 91 (17) (2007) 173108, https://doi.org/10.1063/1.2800796.

[10] M. Vandescuren, P. Hermet, V. Meunier, L. Henrard, P. Lambin, Theoretical study of the vibrational edge modes in graphene nanoribbons, Phys. Rev. B 78 (2008) 195401, https://doi.org/10.1103/PhysRevB.78.195401. https://link.aps.org/doi/10.1103/PhysRevB.78.195401.

[11] M. Yamada, Y. Yamakita, K. Ohno, Phonon dispersions of hydrogenated and dehydrogenated carbon nanoribbons, Phys. Rev. B 77 (2008), 054302, https://doi.org/10.1103/PhysRevB.77.054302. https://link.aps.org/doi/10.1103/PhysRevB.77.054302.

[12] J. Zhou, J. Dong, Radial breathing-like mode of wide carbon nanoribbon, Phys. Lett. A 372 (48) (2008) 7183–7186, https://doi.org/10.1016/j.physleta.2008.10.059. http://www.sciencedirect.com/science/article/pii/S0375960108015429.

[13] R. Gillen, M. Mohr, C. Thomsen, J. Maultzsch, Vibrational properties of graphene nanoribbons by first-principles calculations, Phys. Rev. B 80 (2009) 155418, https://doi.org/10.1103/PhysRevB.80.155418. https://link.aps.org/doi/10.1103/PhysRevB.80.155418.

[14] R. Gillen, M. Mohr, J. Maultzsch, Raman-active modes in graphene nanoribbons, Phys. Status Solidi B 247 (2010) 2941–2944, https://doi.org/10.1002/pssb.201000354. https://onlinelibrary.wiley.com/doi/abs/10.1002/pssb.201000354.

[15] R. Gillen, M. Mohr, J. Maultzsch, Symmetry properties of vibrational modes in graphene nanoribbons, Phys. Rev. B 81 (2010) 205426, https://doi.org/10.1103/PhysRevB.81.205426. https://link.aps.org/doi/10.1103/PhysRevB.81.205426.

[16] D. Liu, A.G. Every, D. Tománek, Continuum approach for long-wavelength acoustic phonons in quasi-two-dimensional structures, Phys. Rev. B 94 (2016) 165432, https://doi.org/10.1103/PhysRevB.94.165432. http://link.aps.org/doi/10.1103/PhysRevB.94.165432.

[17] C. Ma, L. Liang, Z. Xiao, A.A. Puretzky, K. Hong, W. Lu, V. Meunier, J. Bernholc, A.-P. Li, Seamless staircase electrical contact to semiconducting graphene nanoribbons, Nano Lett. 17 (10) (2017) 6241–6247, https://doi.org/10.1021/acs.nanolett.7b02938.

[18] G. Borin Barin, A. Fairbrother, L. Rotach, M. Bayle, M. Paillet, L. Liang, V. Meunier, R. Hauert, T. Dumslaff, A. Narita, K. Müllen, H. Sahabudeen, R. Berger, X. Feng, R. Fasel, P. Ruffieux, Surface-synthesized graphene nanoribbons for room temperature switching devices: substrate transfer and ex situ characterization, ACS Appl. Nano Mater. 2 (4) (2019) 2184–2192, https://doi.org/10.1021/acsanm.9b00151.

[19] S. Zhao, G. Borin Barin, L. Rondin, C. Raynaud, A. Fairbrother, T. Dumslaff, S. Campidelli, K. Müllen, A. Narita, C. Voisin, P. Ruffieux, R. Fasel, J.-S. Lauret, Optical investigation of on-surface synthesized armchair graphene

nanoribbons, Phys. Status Solidi B 254 (11) (2017) 1700223, https://doi.org/10.1002/pssb.201700223. https://onlinelibrary.wiley.com/doi/abs/10.1002/pssb.201700223.

[20] L. Talirz, H. Söde, T. Dumslaff, S. Wang, J.R. Sanchez-Valencia, J. Liu, P. Shinde, C.A. Pignedoli, L. Liang, V. Meunier, N.C. Plumb, M. Shi, X. Feng, A. Narita, K. Müllen, R. Fasel, P. Ruffieux, On-surface synthesis and characterization of 9-atom wide armchair graphene nanoribbons, ACS Nano 11 (2) (2017) 1380–1388, https://doi.org/10.1021/acsnano.6b06405.

[21] J.P. Llinas, A. Fairbrother, G.B. Barin, W. Shi, K. Lee, S. Wu, B.Y. Choi, R. Braganza, J. Lear, N. Kau, W. Choi, C. Chen, Z. Pedramrazi, T. Dumslaff, A. Narita, X. Feng, K. Müllen, F. Fischer, A. Zettl, P. Ruffieux, E. Yablonovitch, M. Crommie, R. Fasel, J. Bokor, Short-channel field-effect transistors with 9-atom and 13-atom wide graphene nanoribbons, Nat. Commun. 8 (2017) 633, https://doi.org/10.1038/s41467-017-00734-x.

[22] Z. Chen, H.I. Wang, N. Bilbao, J. Teyssandier, T. Prechtl, N. Cavani, A. Tries, R. Biagi, V. De Renzi, X. Feng, M. Kläui, S. De Feyter, M. Bonn, A. Narita, K. Müllen, Lateral fusion of chemical vapor deposited n = 5 armchair graphene nanoribbons, J. Am. Chem. Soc. 139 (28) (2017) 9483–9486, https://doi.org/10.1021/jacs.7b05055.

[23] J. Overbeck, G. Borin Barin, C. Daniels, M. Perrin, L. Liang, O. Braun, R. Darawish, B. Burkhard, T. Dumslaff, X.-Y. Wang, A. Narita, K. Müllen, V. Meunier, R. Fasel, M. Calame, P. Ruffieux, Optimized substrates and measurement approaches for Raman spectroscopy of graphene nanoribbons, arXiv:1907.01797, https://arxiv.org/abs/1907.01797, 2019.

[24] Supplementary Material contains a comparison between different scaling functions used to describe the frequency-width relationship in graphene nanoribbons and shows atomic displacements in breathing modes of circular graphene discs, This information is provided free of charge at the URL, https://journals.aps.org/prb/XXXX/2DRBLM19-SM.pdf.

[25] D.W. Brenner, O.A. Shenderova, J.A. Harrison, S.J. Stuart, B. Ni, S.B. Sinnott, A second-generation reactive empirical bond order (REBO) potential energy expression for hydrocarbons, J. Phys. Condens. Matter 14 (4) (2002) 783–802, https://doi.org/10.1088/0953-8984/14/4/312.

[26] R.C. Andrew, R.E. Mapasha, A.M. Ukpong, N. Chetty, Mechanical properties of graphene and boronitrene, Phys. Rev. B 85 (2012) 125428, https://doi.org/10.1103/PhysRevB.85.125428. https://link.aps.org/doi/10.1103/PhysRevB.85.125428.

[27] S. Bashmal, R. Bhat, S. Rakheja, Frequency equations for the in-plane vibration of circular annular disks, Adv. Acoust. Vib. 2010 (2010) 501902, https://doi.org/10.1155/2010/501902.

[28] J.L. Rose, Ultrasonic Waves in Solid Media, Cambridge University Press, 2004. Ch. 11.

[29] D. Tománek, A. Kyrylchuk, Designing an all-carbon membrane for water desalination, Phys. Rev. Appl. 12 (2019), 024054, https://doi.org/10.1103/PhysRevApplied.12.024054. https://link.aps.org/doi/10.1103/PhysRevApplied.12.024054.